Soft Matter

RSC Publishing

PAPER

View Article Online
View Journal | View Issue

Quiescent bilayers at the mica–water interface†

Cite this: *Soft Matter*, 2013, **9**, 7028

Francesca Speranza,[a] Georgia A. Pilkington,[a] Thomas G. Dane,[a] Philip T. Cresswell,[a] Peixun Li,[b] Robert M. J. Jacobs,[c] Thomas Arnold,[d] Laurence Bouchenoire,[ef] Robert K. Thomas[b] and Wuge H. Briscoe*[a]

Despite extensive studies with many experimental techniques, the morphology and structure of the self-assembled aggregates of *quaternary alkyl ammonium bromides* (C_nTABs; where n denotes the number of hydrocarbons in the surfactant tail) at the solid–liquid interface remains controversial, with results from atomic force microscopy (AFM) imaging pointing to a variety of surface aggregates such as cylinders and surface micelles, whilst surface force measurements and neutron reflectivity (NR) measurements reporting bilayer structures. Using a home-built liquid cell that employs the "bending mica" method, we have performed unprecedented synchrotron X-ray reflectometry (XRR) measurements to study the adsorption behaviour of a C_nTAB series (n = 10, 12, 14, 16 and 18) at the mica–water interface at different surfactant concentrations. We find that our XRR data cannot be described by surface aggregates such as cylindrical and spherical structures reported by AFM studies. In addition we have observed that the bilayer thickness, surface coverage and the tilt angle all depend on the surfactant concentration and surfactant hydrocarbon chain length n, and that the bilayer thickness reaches a maximum value at approximately the critical micellisation concentration (~1 cmc) for all the C_nTABs investigated. We propose that C_nTABs form disordered bilayer structures on mica at concentrations below cmc, whilst at ~1 cmc they form more densely packed bilayers with the tails possibly tilted at an angle θ_t ranging from ~40 to 60° with respect to the surface normal in order to satisfy the packing constraints due to the mica lattice charge, *i.e.* so that the cross-section area of the tilted chain would match that of the area of the lattice charge ($A_s \cong 46.8$ Å^2). As the surfactant concentration further increases, we find that the bilayer thickness decreases, and we ascribe this to the desorption of surfactant molecules, which recovers certain disorder and fluidity in the chain and thus leads to interdigitated bilayers again. In light of our XRR results, previously unattainable at the mica–water interface, we suggest that the surface aggregates observed by AFM could be induced by the interaction between the scanning probe and the surfactant layer, thus representing *transient* surface aggregation morphologies; whereas the C_nTAB bilayers we observe with XRR are intrinsic structures under *quiescent* conditions. The suggestion of such *quiescent bilayers* will have fundamental implications to processes such as lubrication, self-assembly under confinement, detergency and wetting, where the morphology and structure of surfactant layers at the solid–liquid interface is an important consideration.

Received 31st January 2013
Accepted 25th April 2013

DOI: 10.1039/c3sm50336d

www.rsc.org/softmatter

1 Introduction

Surfactants and amphiphilic molecules can readily adsorb at the solid–aqueous interface and form various organized structures. Understanding the characteristics of such adsorbed molecular structures and their properties is important to many chemical and industrial applications and processes. One of the most utilized model hydrophilic surface in related fundamental studies is *muscovite mica* (formula unit $KAl_2(Si_3Al)O_{10}(OH)_2$). Due to its easily achievable molecular smoothness, mica is an ideal substrate for AFM,[1–17] surface force apparatus SFA[18–30] and electron microscopy (EM)[31] measurements. Among the most extensively studied cationic surfactants are the C_nTABs and their adsorption at solid–liquid interface has been

[a]*School of Chemistry, University of Bristol, Cantock's Close, Bristol BS8 1TS, UK. E-mail: wuge.briscoe@bris.ac.uk; Fax: +44 (0)117 925 1295; Tel: +44 (0)117 3318256*
[b]*Physical and Theoretical Chemistry Laboratory, University of Oxford, South Parks Road, Oxford OX1 3QZ, UK*
[c]*Department of Chemistry, Chemistry Research Laboratory, University of Oxford, Mansfield Road, Oxford OX1 3TA, UK*
[d]*Diamond Light Source Ltd., Diamond House, Harwell Science and Innovation Campus, Didcot, Oxfordshire, OX11 0DE, UK*
[e]*XMaS, The UK-CRG, European Synchrotron Radiation Facility (ESRF), 6 Rue Jules Horowitz, BP 220, 38043 Grenoble CEDEX 9, France*
[f]*Department of Physics, Oliver Lodge Laboratory, University of Liverpool, Oxford Street, Liverpool L69 7ZE, UK*

† Electronic supplementary information (ESI) available. See DOI: 10.1039/c3sm50336d

characterized in detail by many experimental techniques, including AFM,[2,3,6–14,16,17,32,33] SFA,[21–25,27,34,35] neutron reflectivity (NR),[33,37–40] optical reflectivity (OR),[32,41–43] ellipsometry,[44,45] calorimetry,[46,47] Fourier transform infrared (FTIR) spectroscopy,[48,49] X-ray photoelectron spectroscopy (XPS)[50] and simulation studies.[51–55]

The SFA was among the first techniques applied in order to determine the thickness of the adsorbed surfactant films. In 1981 by Pashley and Israelachvili[23] investigated the adsorption of C_{16}TAB on mica. They observed the formation of a monolayer at a concentration of 1/20 critical micellar concentration (*i.e.* 0.05 cmc), and a second layer to adsorb atop the first layer near the cmc, giving a bilayer of a total thickness 3.2 ± 0.2 nm. However, in a follow-up experiment conducted by the authors[24] these observations above cmc were not reproduced, suggesting possible contamination in the original study. After this pioneering work, a number of SFA studies on the adsorbed layers of C_nTABs ensued.[21,22,25,27,34] For example, in 1989 Kékicheff *et al.* reported *cetyltrimethylammonium bromide* (C_{16}TAB) to form a stable bilayer structure at ~0.5 cmc, with a thickness of approximately 3.2 nm.[21] Such a thickness value is in agreement with the range between 3.1 and 3.6 nm obtained by a number of studies, including those by Israelachvili, Pashley and coworkers,[23–25,34] Helm *et al.*[27] and Richetti and Kekicheff.[22]

On the other hand, AFM imaging has shown different adsorption mechanisms, unveiling a number of aggregate morphologies of C_nTABs adsorbed on different substrates, ranging from spheres to cylinders. For example, in an AFM study of the adsorption of C_{14}TAB by Manne and Gaub,[3] direct images of different surfactant aggregates on a number of solid surfaces were obtained in aqueous solutions. On silica and graphite, spherical admicelles with no long-range order and hemi-cylindrical structures were observed, respectively; whereas on a mica substrate the adsorbed structures consisted of meandering stripes, separated by 5.3 nm, which were suggested to be full cylindrical aggregates with possibly flattened bottom to allow a greater contact area between headgroups and the surface.

Ducker *et al.*[2,6,7] have also investigated the adsorption mechanism of C_{16}TAB at the mica–solution interface using AFM imaging. The initial organization of the surfactant aggregates (at 2 cmc) was found to be in the form of flattened parallel cylinders, with a diameter of about 7 nm,[6] similar to those reported by Manne and Gaub.[3] After approximately 24 h, the adsorbed layer structures were then seen to transform into a flat bilayer. This shape transition was attributed to slow exchange of $C_{16}TA^+$ for the K^+ ions in the mica sites. Further to these observations, the addition of KBr and HBr was also found to transform the stable flat C_{16}TAB sheet to cylinders and then defective cylindrical structures as salt concentration increased. Moreover, Lamont and Ducker proved that several alkali cations, such as K^+, Cs^+ and Li^+, caused shape transitions in the adsorbed aggregate layers. For instance, Cs^+ ion was shown to alter the adsorbed $C_{16}TA^+$ bilayer structure into cylinders and spheres as its concentration was increased.[7] Two possible explanations were proposed for the effect of salt addition: (i) the electrolyte cations compete with surfactant cations for charged mica lattice sites at high salt concentration, or (ii) the binding of the free counterions to the surfactant headgroups could lower the tendency of the surfactant to bind to the surface.[6]

In a later study, Liu and Ducker also investigated the effect of temperature on the geometry of several adsorbed C_nTABs on mica, silica and graphite.[2] AFM measurements were made below and above the bulk Krafft temperatures (T_K) of the surfactants. Below T_K, they found that C_{16}TAB formed flat layer which was 2.4 nm in thickness on mica, indicative of interdigitated surfactant chains. However, above T_K, C_{16}TAB was initially found to form cylindrical aggregates, which gradually transformed into flat structures 4.3 nm thick over a period of ~17 h.

In 2001, using AFM, Subramanian and Ducker[56] also measured the force between a glass particle and a silica substrate in aqueous C_{12}TAB solutions as a function of surface separation and surfactant concentration. The resultant force was related to surface excess of $C_{12}TA^+$ using a Maxwell relation:

$$\left(\frac{F}{\mu_i}\right)_{T,p,\mu_j,s} = 2\left(\frac{n_i}{s}\right)_{T,p,\mu_i,\mu_j} \quad (1)$$

where F is the repulsive force between two identical surfaces at equilibrium, μ_i is the chemical potential of the i^{th} component of the solution, n_i is the surface excess of component i for each surface, and s is the separation between the colloidal particle and the substrate.

This equation states that the change in the force between two surfaces when a surface-active element is added to the solution is related to the change in surface excess as a function of the surface separation. Such change in adsorption with surface separation is denoted as "*proximal adsorption*" since the adsorbed amount is dependent on the proximity of two surfaces. At low surfactant concentrations, the authors found the surfactant adsorbed to the surfaces as they approached. In the range of concentration 1/130–1/10 cmc, and for separations greater than about 10 nm, the adsorption was independent of surface separation. However, when the surface separation decreased from 7 nm to contact the adsorbed amount significantly increased. At higher C_{12}TAB concentrations of 1–10 cmc, surfactant monomers were found to desorb from the surfaces as they approached to reduce the electrostatic repulsion between the surfaces. In a further study by Lokar and Ducker,[57] upon addition of 20 mM KBr, the onset separation for separation-dependent adsorption was found to be reduced, and adsorption depended on the surface charge. That is, as the surfaces approached each other, more surfactant monomers would adsorb if the interacting surfaces were negatively charged, whereas they would desorb when the interacting surfaces were positively charged.

In an earlier study, Podgornik and Parsegian[58] analysed surface force data between mica surfaces in C_{16}TAB solutions and showed the existence of puzzling long-range attractive forces. Some measurements of such additional force could be explained by the inter-dependence of force and C_{16}TAB adsorption. Furthermore, Yaminsky *et al.*[59–61] have also used the proximal adsorption analysis to explain force measurements between silica substrates in C_{16}TAB. These force measurements using AFM and

SFA suggest that the adsorbed surface layers would become perturbed by a second surface in the proximity, imparted by the inter-surface interactions. Such a perturbation was also suggested by Subramanian and Ducker[56] in an AFM imaging study of the morphology of the adsorbed C_{12}TAB layer structure at the silica–solution interface. In the surfactant concentration range 0.1–0.5 cmc, they observed a featureless layer; whereas, from 0.5 to 39 cmc, cylindrical structures were observed, consistent with either spheres or hemispheres atop a monolayer. A possible consequence of the proximal adsorption arguments is that the presence of an imaging AFM tip may induce a dramatic change in the adsorbed amount of the surfactant, and hence, also in their surface aggregate morphology.

Many neutron reflectivity (NR) studies have also investigated the structures of C_nTABs on silica[37–39] and quartz.[33,40] Most of these studies have shown that the adsorption of C_nTABs occurs in the form of patchy bilayer aggregates, differing from the morphology by AFM studies. For instance, in 1990 Rennie *et al.*[38] found that the surface coverage of adsorbed C_{16}TAB layers increased from 35% at 1/3 cmc to 80% at 2/3 cmc and the layer thickness to be 34 Å, consistent with either a defective bilayer or flattened micelles on silica. Similar results were also obtained for the adsorption of C_{16}TAB on quartz by McDermott *et al.*:[40] at 1/3 cmc the C_{16}TAB surface coverage was found to be 51%, whereas at 1 cmc this increased to 65%. However, at both concentrations the adsorbed layer thickness of 34 Å was measured. Thirdly, these results have also been confirmed by Fragneto *et al.*[37] who studied the C_{16}TAB structure on smooth and rough silicon surfaces. In agreement with the studies above, their results support the idea that C_{16}TAB absorption occurs *via* the formation of bilayer fragments, and the surface is not fully covered. Furthermore, the layer thickness measured, was found to be 32 Å, indicating that the bilayers were either interdigitated or strongly tilted.

The adsorption kinetics of C_nTABs on silica has also been investigated by optical reflectometry (OR) studies.[32,41–43] For example, in 1998 Pagac *et al.*[41] investigated the adsorption kinetics of C_{16}TAB on silica using OR. They found that the initial adsorption rate of C_{16}TAB increased as its concentration was increased between 0.2 cmc and 10 cmc, although a discontinuity at the cmc was noted. Moreover, an adsorption maximum below the cmc, which was then followed by a decrease in C_{16}TAB adsorption, reaching a plateau which continued at concentrations well above the cmc was also observed. Their kinetic data indicates a change in the adsorption mechanism and in the structure of the adsorbed layer at the cmc. That is, below the cmc, monomeric surfactant molecules adsorbed on the substrate, forming a defective bilayer. However, above the cmc, micelles adsorbed directly onto the surface, leading to a closely packed monolayer of micelles. In a later study, Atkin *et al.*[43] examined the adsorption of C_{16}TAB to the silica–water interface as a function of C_{16}TAB concentration, with and without added salt, and as a function of pH. At the critical surface aggregation concentration of C_{16}TAB they observed a very slow adsorption process that was interpreted as resulting from a slow structural change in the adsorbed surfactant film. In contrast, the adsorption was completed very quickly (within minutes) at all other concentrations, below and above the cmc, as well as in the presence of 10 mM KBr. Such results suggest that, at concentrations above the cmc, complete micelles participated in the adsorption process, in agreement with the work of Pagac *et al.*[41]

As well as surfactant and electrolyte concentration, the influence of counterion identity on the morphology of adsorbed aggregates of C_{16}TAB has been studied on silica by Velegol *et al.*,[32] using both OR and AFM. The results from both techniques suggest a change in the $C_{16}TA^+$ adsorption behaviour near the cmc. AFM imaging showed that when the C_{16}TAB concentration was increased from 0.9 cmc to 10 cmc the adsorbed aggregate morphology changed from very short rods to long cylindrical structures. This result remained the same in the presence of 10 mM KBr, although added electrolyte reduced the spacing between the surface aggregates. Alternatively, in the presence of a Cl^- counterion, C_{16}TAC was found to form spherical aggregates at both surfactant concentrations. These structures were again found to be stable in the presence of KBr. From the above studies, the effect of surface charge density of the substrate may be appreciated by comparing the adsorption behaviour and aggregate morphologies on silica and mica surfaces. Due to the lower charge density of silica compared to mica, the following trend has been observed: an increase in the spacing between wormlike C_{16}TAB aggregates, greater axial curvature of adsorbed C_{16}TAB cylindrical aggregates, and a greater sensitivity of the structure of $C_{16}TA^+$ aggregates to the counterion binding efficiency on silica than on mica.

Recently, several computer simulation studies have also probed the molecular organization of soft matter structures adsorbed on hydrophilic surfaces.[51–55] For example, Johnson and Nagarajan[52] modelled the self-assembly of the cationic C_{12}TAB at the solid–liquid interface. In this study they suggested the formation of new composite surface structures. Common to each structure was a monolayer oriented with surfactant head groups in contact with the hydrophilic surface. On top of this monolayer hemispheres, hemicylinders or another monolayer with opposite molecular orientation were observed, *i.e.* bilayers were formed. The energies required for the formation of such composite structures were calculated to be lower than the energies for the self-assembly of the full cylinders or full spheres. Hence, such aggregates were found to be never energetically favoured. These new surface structures obtained from simulation studies are in agreement with previous NR and OR studies, but represent a contrast to the organisation of surfactant aggregates proposed in the AFM literature. Instead, they suggest that the structures observed by AFM experiments may not be cylinders or spheres, but correspond to composite structures made up of hemispheres or hemicylinders atop an underlying monolayer.

In summary, the morphology and structure of the self-assembled surfactant aggregates at the interface remains controversial and the adsorption mechanism is yet to be fully understood, despite extensive related studies. In general, comprehensive NR results suggest bilayer or bilayer-like structures at the silica–water interface, whilst in contrast AFM imaging suggests a variety of surface morphologies which are dependent on a wide range of experimental parameters on both mica and silica.

Hitherto, reflectivity measurements have not been routinely performed at the mica–water interface due to insufficient flatness over a relatively large area as required by such studies – both NR or XRR, as we have previously elaborated in some detail.[62] A recently developed simple technique employing the "bending mica" method has enabled XRR to be applied to study soft matter nanofilms at the mica–water interface.[63] In this study, and by employing this method, we report for the first time XRR results on the adsorption behaviour of a C_nTAB series ($n = 10$, 12, 14, 16 and 18) at different surfactant concentrations at the highly charged mica–water interface. We find that our XRR results cannot be described by the surface aggregate morphologies obtained from AFM imaging. Instead, our results are in a broad agreement with the NR results, and C_nTABs are found to form bilayer-like structures, with the surfactant chains tilted with respect to the surface normal at ~1 cmc. In light of our results and the above review of recent literature, we suggest that surfactants would form bilayers under *quiescent* conditions akin to NR and XRR measurements, whilst the surface aggregates observed with AFM might be *transient* and induced by the interactions between the AFM tip and the surface layer.

2 Materials and methods

2.1 Materials and sample preparation

All the cationic *quaternary alkyl ammonium bromide* surfactants (C_nTABs) with even numbered hydrocarbon chains ($n = 10$, 12, 14, 16 and 18) were synthesised as reported previously.[64] Their abbreviations, molecular formulae and their physical properties (*i.e.* the molar mass (MW), cmc's, and Krafft temperatures (T_K)) are listed in Table 1. Fig. 1(a) shows the molecular structure of the C_{16}TAB surfactant studied as an example. Five different concentrations of all the five surfactants were studied: 0.1, 0.5, 1, 3 and 5 cmc. For the C_{12}TAB surfactant, 0.33 cmc instead of 0.1 cmc was studied, as specified. The C_nTAB solutions used for these measurements were prepared by dissolving appropriate amounts of the surfactants into Ultrapure Milli-Q® water with a conductivity of 18.2 MΩ cm^{-1} at 25 °C.

Bare mica substrates were used for the C_nTAB adsorption studies. Natural muscovite mica (A1 special grade) with composition $KAl_2(Si_3Al)O_{10}(OH)_2$ was purchased from SJ Trading®, New York, in form of thick sheets around 25 × 15 cm in size and 1 mm in thickness. They were cut into smaller pieces for easy handling; then cleavage was initiated by inserting a sharp needle into the edge of the sheet. Sheets of 1 × 3 cm ($w \times l$) in size and 30–100 μm in thickness were cut out of a single sheet to expose a molecularly smooth, fresh 001 crystal surface. The entire preparation process was carried out in a laminar flow hood and polyethylene gloves were worn while mica was handled, and contact of the mica 001 facet with any foreign objects (fingers, tools, glassware, *etc.*) was strictly avoided.

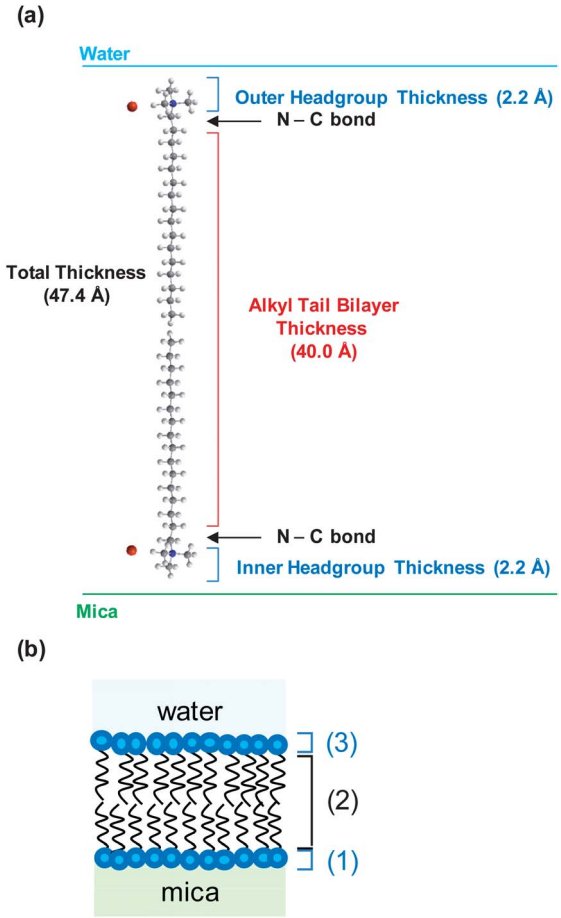

Fig. 1 (a) Molecular dimensions of the headgroups and alkyl tail bilayer of the C_{16}TAB molecule obtained from Chem3D Pro 12.0. The total thickness is calculated including the two N–C bonds between the headgroup and the tail. The thicknesses of other C_nTAB bilayers are calculated similarly. (b) The three-layer model used to model the C_nTAB surfactants bilayer.

Table 1 Molar mass (MW), cmc's, Krafft temperatures (T_K), and fitting parameters for the C_nTAB surfactants studied. (‡) Data by P. Li obtained at Diamond I07 Chemistry Lab. (*) Calculated from Tanford's formula;[36] (⊥) calculated from Gaussian

C_nTAB	M_w (g mol^{-1})	cmc (mM)	Krafft temperature T_K (°C)	Molecular fragment	Fragment molecular formula	Molecular volume V (Å^3)	Total no. of electrons n_e
				Headgroup	$N(CH_3)_3^+$	130*	33
				Counterion	Br^-	37$^\perp$	36
C_{10}TAB	280.29	68.0[1]	<25	Tail	$CH_3(CH_2)_9$	296*	81
C_{12}TAB	308.34	16.0[1]	<25	Tail	$CH_3(CH_2)_{11}$	350*	97
C_{14}TAB	336.39	3.6[1]	<25	Tail	$CH_3(CH_2)_{13}$	404*	113
C_{16}TAB	364.45	0.98[1]	25‡	Tail	$CH_3(CH_2)_{15}$	458*	129
C_{18}TAB	392.50	0.34[1]	36‡	Tail	$CH_3(CH_2)_{17}$	512*	145

2.2 X-ray reflectometry measurements

Using the liquid cell[63] shown in Fig. 2(b) we have performed XRR measurements on beamlines BM28 (XMaS)[65] at the European Synchrotron Radiation Facility (ESRF), and I07 at the Diamond Light Source, UK. A schematic of the X-ray reflectivity experimental setup is shown in Fig. 2(a). A monochromatic incident X-ray beam strikes the sample surface along the bending axis of the mica sheet at some known grazing angle θ_i (varying from 0.06° to 2.4° in our experiments), corresponding to a range (0.014–0.6 Å^{-1}) of the vertical momentum transfer vector Q ($=4\pi\sin\theta/\lambda$). For the measurements performed at beamline ESRF BM28, the incident beam size defined by slits was 300 (vertical) × 300 μm (horizontal) with an incident flux of ~10^6 photons per s. The BM28 monochromator was tuned to select an X-ray beam energy of 14.0 keV with a corresponding wavelength $\lambda = 0.886$ Å. Two different experiments were carried out at beamline I07, Diamond. X-ray beam energies of 20.0 keV ($\lambda = 0.619$ Å) and 23.0 keV ($\lambda = 0.539$ Å) were used. The incident beam sizes defined by slits were 130 μm (vertical) × 320 μm (horizontal) and 220 μm (vertical) × 250 μm (horizontal), respectively. In each measurement, we first collected the specular reflection (*i.e.* $\theta_i = \theta_r$; *cf.* Fig. 2), then the off-specular diffuse scattering was collected for each scan with identical parameters by detuning the incident angle by 0.06–0.1° (chosen according to the alignment rocking curves) on either side of θ_i but with half the integration time of that of the specular reflectivity. The final reflectivity was obtained by subtracting the diffuse scattering from the specular reflectivity. Collecting one full dataset, for both specular and off-specular scans, requires around 2 hours, whilst alignment takes ~2 to 6 hours for an initial bare mica sheet.

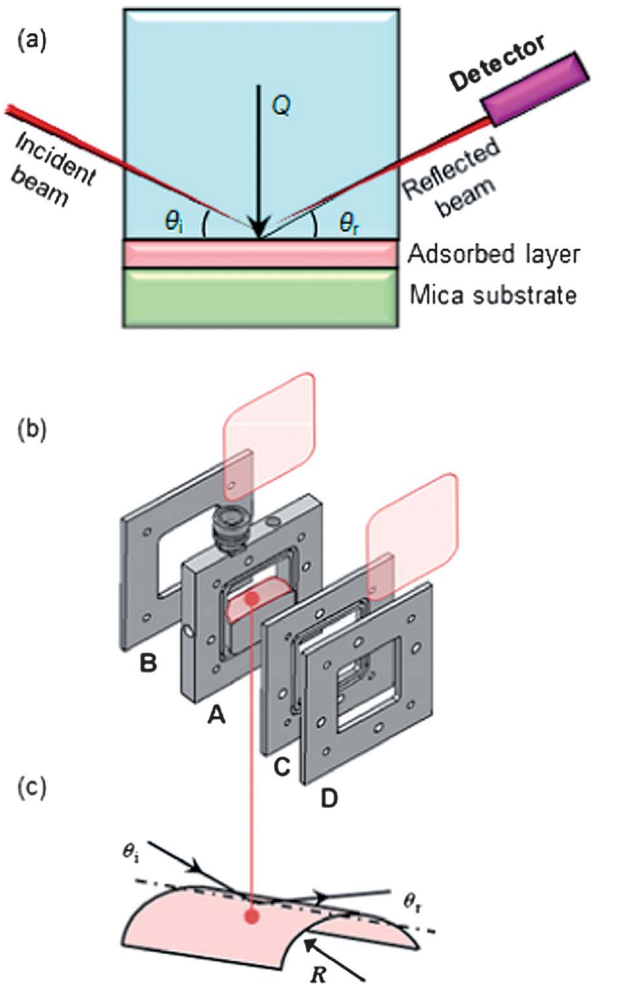

Fig. 2 (a) Schematic of the XRR experimental setup. (b) Key components of the liquid cell, consisting of four stainless steel plates (A–D). Two mica windows of ~100 μm thick and ~45 × 45 μm in size are clamped between plates C and D, and then onto plate A, with a liquid chamber formed when a second mica window is clamped between plates A and B. (c) The geometry of the bending mica method, with θ_i, θ_r, and R (~7.5 cm) the incidence angle, the reflected angle and the bending radius respectively.

A freshly cleaved mica sheet was mounted in the liquid cell, where it was slightly bent and clamped over an underlying cylinder.[62,63] The liquid cell was mounted to the stage of a Huber diffractometer and the C_nTAB surfactant solution was injected into the cell. C_{10}TAB to C_{14}TAB series measurements were made at room temperature (21 °C). C_{16}TAB and C_{18}TAB measurements were made at 45 °C, *i.e.* above their Krafft temperatures. To achieve such temperatures, two DBK® positive temperature coefficient (PTC) heaters were attached to the outside faces of plates B and D of the liquid cell (*cf.* Fig. 2(b)). Whilst the temperature of the cell was constantly monitored by a thermocouple, which was also mounted (away from the heaters) on the outside face of one of plates B or D.

2.3 Data analysis and fitting model

For the data analysis we have taken into account the effect of the crystal truncation rods (CTR) due to mica's layered crystal structure on the overall reflectivity. Some considerations and an overview our data analysis approach have been described previously.[63]

Data fitting is performed with a Java™ based software package using the standard matrix algorithm, in which the interface region is modelled as a series of homogeneous, planar layers. Each layer is characterised by its scattering length density (SLD) ρ, thickness t, and an interfacial roughness factor. By varying ρ as well as t for each layer, the calculated reflectivity profile may be compared with the experimental profile until an optimum fit is achieved.

This procedure eliminates any possible skewing effect by the presence of the forbidden peak, and allows us to judiciously focus on the main features of the Kiessig fringes. For instance, the data points below the critical edge are typically inaccurate due the edge effect of the mica sheet at such low incident angles, and we do not focus on fitting this segment of the curve. The software also contains a constraint so that the stoichiometry of the layers is correct as these parameters are varied, *i.e.* it does not permit unphysical fitting results, such as >100% volume fractions.

C_nTAB thin film systems have been modelled using different layer components on the basis of their own structural features. Every C_nTAB surfactant molecule is divided into three fragments: the hydrophobic tail, the hydrophilic headgroup and the

counterion. As aforementioned, the C_nTABs used in this study only differ in the length of their hydrocarbon chains, whereas the cationic headgroup and the anionic counterion are identical for all the surfactant molecules, *i.e.* quaternary ammonium cation ($N(CH_3)_3^+$) and bromide (Br^-), respectively. The parameters required in fitting the data, *i.e.* the total number of electrons n, and the molecular volumes V for each of the above layers, are listed in Table 1. The molecular volumes were estimated using the Tanford's formula[36] or the software Gaussian® 03W (Gaussian Inc.).

For every C_nTAB, the surfactant bilayer has been modelled using a three-layer model as schematically shown in Fig. 1(b), in the sequence of their proximity to the mica surface: (1) the inner headgroup layer, $N^+(CH_3)_3$; (2) the hydrocarbon chain segment, $CH_3(CH_2)_{n-1}$; (3) the outer headgroup layer, $N^+(CH_3)_3$; and water as superphase. In addition, the fractions of the inner and outer headgroups associated with the counterions, Br^-, were also allowed to vary.

The fitting programme yields the thickness t, the surface coverage and the roughness of each layer, as well as the fractions of the inner and outer headgroups associated with counterions. The parameters obtained from the fit of all the C_nTABs (n = 10, 12, 14, 16 and 18) studied at the five different concentrations are listed in Tables 2 and 3, and in Tables S1–3 of the ESI†. The *Tanford's chain length*, l_c, was estimated using the Tanford's relation,[36] whereas the *calculated thickness*, t_c, was obtained from the dimensions of the surfactant molecules in Chem3D Pro 12.0 (CambridgeSoft). The calculated thickness of the alkyl tail bilayer was determined assuming fully extended bilayer, and the total thickness includes the N–C bond between the headgroup and the tail. This is schematically shown in Fig. 1(a) for the C_{16}TAB molecule as an example. Tables 2 and 3, as well as Tables S1–3 in the ESI† also list t, the *fitted thickness* value, the *fractions of association*, *i.e.* the degrees of association of the inner and outer headgroups with ions, the *roughness*, the *surface coverage* and, finally, the possible bilayer *tilt angle* with respect to (w.r.t.) the surface normal.

3 Results and discussions

3.1 General features in XRR curves and the structures of C_nTAB surface layers

As an example, the results from C_{10}TAB (*cf.* Fig. 3, and Table 2) and C_{16}TAB (*cf.* Fig. 4, and Table 3) are described here in detail. The results from all the other studied C_nTABs have similar features in their XRR curves as shown in ESI Section A.† The differences between C_nTAB surface structures will be described later in the section. Fig. 3 shows the experimental XRR profiles (*i.e.* reflectivity *vs.* Q) from C_{10}TAB adsorbed on mica, along with the corresponding fits (solid red curves), at five different concentrations, *i.e.* 0.1, 0.5, 1, 3 and 5 cmc. In general, the feature (*i.e.* a small peak) at $Q \sim 0.32$ Å^{-1}, half of the Q value for the Bragg peak, in all the curves is the *forbidden peak* due to mica's monoclinic unit cell encompassing two lattice layers and thus its non-unique unit cell assignment.

The fitting parameters, listed in Table 2, show a full coverage of the surface by the alkyl tails above 1 cmc. On the other hand, at 0.1 and 0.5 cmc, lower coverage of 42% and 50% is obtained, respectively, indicating that the surfactant bilayers only exist in patches. The adsorbed surfactant layer thickness (*cf.* column 6 in Table 2) for C_{10}TAB shows a maximum at 1 cmc, and unexpectedly it then decreases at higher surfactant concentrations. Such a maximum in the thickness of the adsorbed layers at ~1 cmc is observed for all the C_nTABs in the series. In addition, the thickness values of all the adsorbed C_nTAB bilayers at all concentrations are found to be less than the length of two fully extended surfactant molecules.

For instance, the thickness of the adsorbed C_{10}TAB bilayer at 1 cmc is found to be 24.1 Å (including the inner and outer headgroups). This value is smaller than the calculated value for

Table 2 Fitting parameters for C_{10}TAB for XRR data shown in Fig. 3. (♯) If tilted bilayers are assumed

Surfactant concentration		Inner headgroup layer	Outer headgroup layer	Alkyl tail bilayer	Total thickness	Roughness at bilayer–water interface (Å)	Coverage (%)
	Tanford's chain length $2l_c$ (Å)			28.3			
	Calculated Thickness t_c (Å)	2.2	2.2	24.7	31.6		
0.1 cmc	Fitted thickness t (Å)	2.2	2.2	17.9	22.3		
	Fraction of association (%)	92	36			2.9	42
	Tilt angle w.r.t. surface normal			45.1°♯			
0.5 cmc	Fitted thickness t (Å)	2.3	2.3	19.1	23.7		
	Fraction of association (%)	100	21			3.0	50
	Tilt angle w.r.t. normal			41.4°♯			
1 cmc	Fitted thickness t (Å)	2.3	2.3	19.5	24.1		
	Fraction of association (%)	98	50			3.0	100
	Tilt angle w.r.t. surface normal			40.3°			
3 cmc	Fitted thickness t (Å)	2.1	2.2	15.5	19.8		
	Fraction of association (%)	96	25			3.0	100
	Tilt angle w.r.t. surface normal			51.2°♯			
5 cmc	Fitted thickness t (Å)	2.3	2.2	16.4	20.9		
	Fraction of association (%)	98	27			3.0	100
	Tilt angle w.r.t. surface normal			48.6°♯			

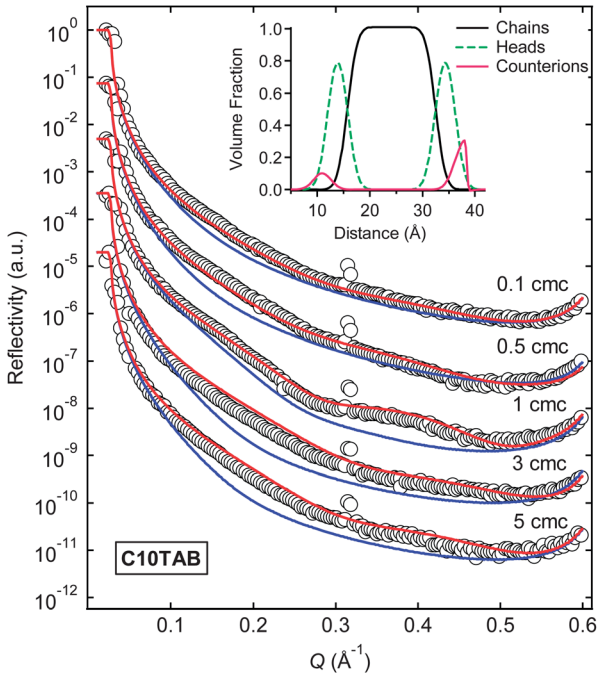

Fig. 3 Experimental (open circles) and fitted (solid red curves) reflectivity curves for C_{10}TAB at five different concentrations (0.1, 0.5, 1, 3 and 5 cmc, as indicated), scaled for clarity. The solid blue curves show the fitted reflectivity when surface cylinders are assumed instead of bilayers. The inset shows the volume fraction profiles of each segment used for fitting the data at 1 cmc, where the zero distance corresponds to the mica surface.

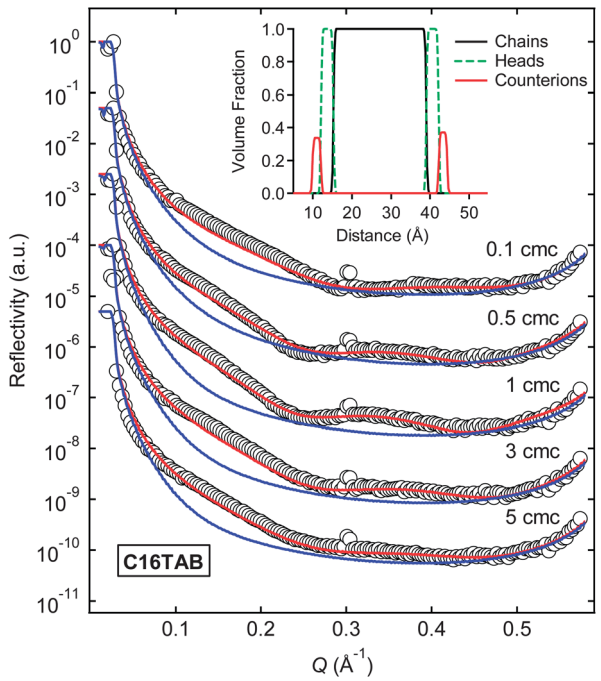

Fig. 4 Experimental (open circles) and fitted (solid red curves) reflectivity curves for C_{16}TAB at five different concentrations (0.1, 0.5, 1, 3 and 5 cmc, as indicated), scaled for clarity. The solid blue curves show the fitted reflectivity when using the corresponding calculated RMS roughness at each concentration. The inset shows the volume fraction profiles of each segment used for fitting the data at 1 cmc, where the zero distance corresponds to the mica surface.

two fully extended C_{10}TAB molecules (~31.6 Å), suggesting possible interdigitation of the alkyl chains, *i.e.* the chains from the proximal and distal leaflets of the bilayer penetrate into each other. An alternative conformation which would also give such a bilayer thickness is one in which the CTAB alkyl tails would tilt to an angle of $\cos^{-1}(24.1/31.6) \approx 40.3°$ with respect to the surface normal. Our simple three-layer model could not directly distinguish between these two possibilities. We will discuss these two possible structures later. It should also be noted that the data could not be fitted using a monolayer model.

We have also attempted to fit the XRR data with the cylindrical structures found by AFM imaging experiments, and in doing so it is pertinent to consider the root mean square (RMS) roughness of surface cylinders or radius R, *i.e.* RMS roughness $= 0.577R$ where $2R \sim t \sim$ 20–24 Å is taken approximately the thickness of the surface layer. Using an RMS roughness in the range 6–7 Å and 100% surface coverage for C_{10}TAB, we have calculated the corresponding XRR profiles, shown as blue curves in Fig. 3, which contrast with the subtle Kiessig fringes in the measured reflectivity data for the C_{10}TAB at five concentrations. It is evident that our XRR data cannot be fitted using such RMS roughness values, indicating that the adsorption surface aggregates could not be in the form of cylindrical structures. Similarly, our data cannot be described by surface micelles. Instead, our results are best described by a bilayer structure, shown as red curves in Fig. 3. We further show that assuming different values for surface coverage and surface roughness in computing XRR profiles cannot describe our data in Fig. S4 in the ESI section.†

It is also worth noting that the inner and outer quaternary ammonium headgroups have different degrees of association, *i.e.* the outer headgroups are found to have a smaller degree of association of the counterions (on average ~30%) than that of the inner headgroups at the mica surface (approaching ~100%). Such findings apply to all the C_nTABs analysed and shown in ESI Section C.†

Another general comment we would like to make is that our bilayer model may not describe the surface structure fully at low surfactant concentrations, where patchy layers or asymmetric bilayers may form. We are most interested in the nanoscale structure of surfactant bilayers, without atomistic details, and the model we have used (*cf.* Fig. 1(b)) and the fits obtained are somewhat crude in comparison with Cheng *et al.*'s crystallographic standards.[66] However, our fits show that the general features of the XRR profiles (*i.e.* the mild Kiessig fringes) can be consistently captured by our simple model. The largest error associated with our measurement concerns the alignment of the incident X-ray beam with the gently curved surface, particularly in the lower angle region. Within the limitations of our model, the relative fitting errors associated with the thickness and surface coverage of the surfactant layers are small, *i.e.* <1%, and the maximum absolute error in all the thicknesses is ±0.2 Å. However, we find the relative errors in the ion fraction are comparatively larger due to the complexity of modelling the ion content and distribution. However, the effect of this error on the calculated profile is secondary, and has little effect on the

Table 3 Fitting parameters for C_{16}TAB for data shown in Fig. 4. (♯) If tilted bilayers are assumed

Surfactant concentration		Inner headgroup layer	Outer headgroup layer	Alkyl tail bilayer	Total thickness	Roughness at bilayer–water interface (Å)	Coverage (%)
	Tanford's chain length $2l_c$ (Å)			43.5			
	Calculated thickness t_c (Å)	2.2	2.2	40.0	47.4		
0.1 cmc	Fitted thickness t (Å)	2.2	2.2	21.8	26.2		
	Fraction of association (%)	100	88			0.5	80
	Tilt angle w.r.t. normal			56.4°♯			
0.5 cmc	Fitted thickness t (Å)	2.2	2.2	26.1	29.9		
	Fraction of association (%)	70	92			0.5	80
	Tilt angle w.r.t. normal			50.9°♯			
1 cmc	Fitted thickness t (Å)	2.2	2.2	25.7	30.1		
	Fraction of association (%)	90	82			0.5	100
	Tilt angle w.r.t. normal			50.5°			
3 cmc	Fitted thickness t (Å)	2.3	2.2	23.0	27.5		
	Fraction of association (%)	92	83			0.5	100
	Tilt angle w.r.t. normal			54.6°♯			
5 cmc	Fitted thickness t (Å)	2.2	2.2	23.9	28.3		
	Fraction of association (%)	95	30			0.5	100
	Tilt angle w.r.t. normal			53.3°♯			

fitted thickness and surface coverage of the surfactant layers. Considering that the ionic layers are less certainly described, the fitting errors in our layer coverage and thickness will increase. But based on trial and error analysis, the relative errors of the fitted layer thickness and coverage will increase to at most 2% and the absolute errors in the thickness to about ±0.3 Å. This is generally true for the fitted parameters listed. This allows scope to refine our physical models in the future, *e.g.* incorporating asymmetric bilayers and a more accurate description of ion distributions at interfaces.

3.2 Further discussions on the structures of different C_nTABs

All of the C_nTABs show similar adsorption behaviour from the C_{10}TAB detailed above in terms of bilayer formation. The fitting parameters for the formation of a C_{12}TAB layer at 1 cmc indicate the formation of a bilayer with full surface coverage and of 25.4 Å in thickness (*cf.* column 6, Table S1 in the ESI†), as the dimension of a fully extended C_{12}TAB molecule is estimated to be ~18.5 Å. For a tilted bilayer, the C_{12}TAB hydrocarbon chains could tilt to an angle of 46°. Overall, these XRR results show a different structural picture from previous AFM studies. For example, Patrick *et al.*[9] observed parallel cylindrical micelles meandering across the surface separated by 4.8 nm in AFM images of C_{12}TAB adsorbed films on mica (at 2 cmc). The morphology of the adsorbed C_{12}TAB layer structure has also been examined at the silica–solution interface by Subramanian and Ducker.[56] A featureless layer was found below cmc (in the concentration range 0.1–0.5 cmc); whereas, from 0.5 to 39 cmc, they observed cylindrical structures consistent with either spheres or hemispheres atop a monolayer. However, in addition to imaging, Subramanian and Ducker[56] also determined the *proximal adsorption* of $C_{12}TA^+$ as a function of the separation between two solid–liquid interfaces (a micron sized glass sphere and a flat silica sheet) and observed that placing another solid surface in contact with a solid–liquid interface caused a dramatic change in adsorption. A possible consequence of this is that the presence of an AFM scanning probe may actually cause a dramatic change in the adsorbed amount of the surfactant, and hence, also in the surface aggregate morphology. Therefore the AFM imaging may not reveal the equilibrium quiescent surface structure formed by surfactants. This will be discussed more in detail later for C_{16}TAB.

As reviewed above in Section 1, Manne and Gaub[3] performed an AFM study of the adsorption of C_{14}TAB on a muscovite mica substrate. They observed that the adsorbed surfactant structures consisted of meandering stripes, suggested to be full cylindrical aggregates. However, Monte Carlo simulation results by Meleshyn[51] indicate that the aggregates arranged as meandering stripes on mica need not necessarily be of a cylindrical shape as suggested by Manne and Gaub.[3] Instead they may represent stripes of a bilayer adsorbed film formed as a consequence of the lateral segregation of hydrophilic and hydrophobic clusters in the interfacial region containing the aliphatic part of the bilayer aggregate. Our results (*cf.* Fig. S1(b)†) do not disagree with the computer simulation studies, showing the formation of a C_{14}TAB bilayer 28.4 Å in thickness, at 1 cmc (*cf.* column 6, Table S2 of the ESI†). If we consider the calculated value for two fully extended C_{14}TAB molecules (~41.6 Å), our results suggest a tilted bilayer (46.9° tilt angle) at 1 cmc, as for the other C_nTABs.

At 0.1 cmc, the fit parameters indicate the formation of a C_{18}TAB adsorbed layer of 27.2 Å in thickness with a surface coverage of 86%. At 1 cmc, a maximum in the adsorbed film thickness of 32.0 Å. The dimension of a fully extended C_{18}TAB molecule is ~25.5 Å, thus it suggests that the C_{18}TAB hydrocarbon tails could be tilted at an angle of $\cos^{-1}(32.0/50.8) \approx 50.9°$ w.r.t. the surface normal. This possibility is supported by a study by Brovelli *et al.*,[67] who examined the orientation of the

C_{18}TAB alkyl chains in self-assembled monolayers on muscovite mica *via* ion exchange using near edge X-ray absorption fine structure spectroscopy (NEXAFS). They found that the alkyl tails either adopted a random orientation, forming a completely disordered layer, or formed an ordered assembly with a specific tilt angle between the chains and the surface normal of 55°. This specific tilt angle has also been observed in molecular dynamics (MD) simulations of C_{18}TAB surfactant adsorption on mica by Heinz *et al.*[55]

3.3 Structure of C_{16}TAB on mica: "*quiescent bilayers*"

C_{16}TAB is among the most studied surfactants, and we thus discuss our C_{16}TAB results in detail in the context of previous findings. Our results show that C_{16}TAB formed bilayers on mica at all five concentrations ranging from 0.1 to 10 cmc. A relatively high coverage (~80%) of the surface by the hydrocarbon chains was observed below the cmc (*cf.* Fig. 5(b)), above the surface coverage was 100%. Moreover, at all concentrations, the outer quaternary ammonium headgroups have a higher degree of association with the counterions at the mica surface (on average ~75%; *cf.* column 4 in Table 3) when compared to the fraction of association of the outer headgroups of the other C_nTABs. At 1 cmc, the thickness of the adsorbed C_{16}TAB bilayer, including the inner and outer headgroups, is found to be 30.1 Å. This value, considerably smaller than two fully extended C_{16}TAB molecules (~47.4 Å), suggests a tilt angle of 50.5° of C_{16}TAB alkyl tails w.r.t. normal.

The adsorption mechanism of C_{16}TAB on muscovite mica has been extensively investigated by Ducker *et al.*[2,6,7] using AFM. They reported the initial organization of the surfactant aggregates in the form of parallel cylindrical structures 35–40 Å in thickness under conditions similar to ours.[6] However, over a period of ~17 h, such aggregates were observed to evolve into flat bilayers, and it was attributed to a slow transport of the inorganic cations out of the surfactant film.[2]

On the other hand, OR studies[41] on silica have reported the formation of defective C_{16}TAB bilayer and nearly close-packed packed monolayer of micelles, below and above the cmc, respectively. Moreover, Atkin *et al.* hypothesized[42,43] that complete micelles participated in the adsorption process, at concentrations above the cmc, in agreement with the work of Pagac *et al.*[41] Their adsorption isotherm, adsorption and desorption kinetics, and concentration-cycling experiments suggested that monomeric surfactant molecules adsorbed on the substrate below the cmc, producing structurally distinct layers. However, above the cmc, micelles were found to adsorb directly to the surface. The greater axial curvature of adsorbed C_{16}TAB cylindrical aggregates on silica was attributed to the lower charge density of silica in comparison to mica.

The thickness of C_{16}TAB aggregates on mica was determined to be ~31 to 36 Å as measured by SFA,[21–25,27,34] which is likely to include the thickness of the hydration layer tenaciously bound to the surfactant headgroups giving rise to the hydration forces between the surfactant bilayers. In agreement with the SFA results, all the NR studies have shown that C_{16}TAB adsorption on silica occurs in the form of patchy bilayer aggregates 32–34 Å in thickness. Thus, our XRR results of C_{16}TAB on mica broadly agree both SFA (on mica) and NR results (on silica), but they all indicate a different picture from that observed in AFM studies.

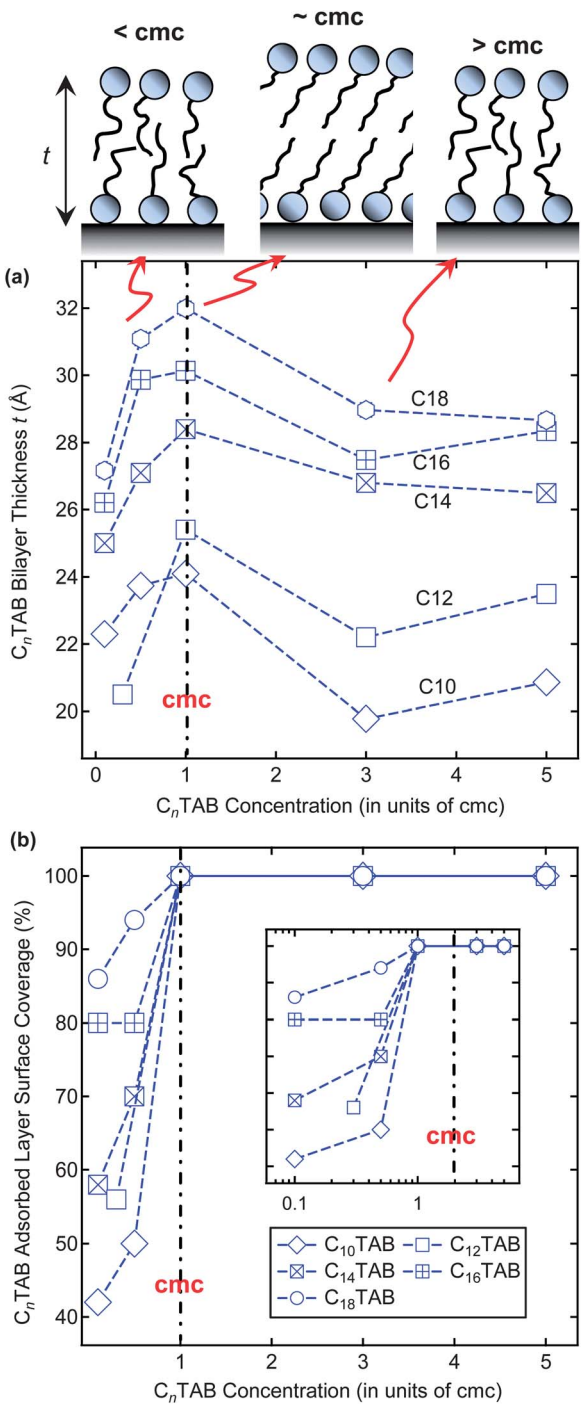

Fig. 5 (a) C_nTAB surfactants bilayer thickness t as a function of surfactant concentration (in units of cmc). All C_nTABs exhibit a maximum t at ~1 cmc. The proposed structures in three different concentration regimes are shown schematically above the figure. The maximum absolute fitting error in all the thicknesses is ±0.2 Å. (b) Surface coverage of C_nTAB layer as a function of surfactant concentration (in units of cmc). The inset is the same plot on a linear-log scale to show more clearly the surface coverage below cmc. The relative fitting errors of the coverage for the surfactant layers are <2%. The symbols have the same meanings in (a) and (b).

The self-assembly behaviour of alkyl ammonium bromide surfactants on a hydrophilic surface has also been modelled by Johnson and Nagarajan.[52] By computing the equilibrium free-energy for the formation of a given structure, they predicted the surface aggregate morphology and proposed the formation of new composite surface structures, as detailed in Section 1. They showed that the formation of such composite structures was energetically more favoured than the full cylinders or spheres. It is evident that these new surface structures obtained from simulation studies are in contrast to the well-known organization of surfactant aggregates proposed in the AFM and OR literature. Their findings indicate that the structures observed by AFM and OR experiments might not be cylinders or spheres, but the corresponding composite structures made up of hemispheres or hemicylinders atop an underlying monolayer. Indeed, AFM measurements are only able to investigate the topology of such adsorbed films. Hence, the identification of full *versus* hemi aggregates is not always definitive.

The fitted roughness of the C_{16}TAB adsorbed layer from our XRR results is small, *i.e.* ~0.5 Å, at all surfactant concentrations. On the other hand, the formation of cylindrical aggregates or admicelle structures would give a much higher RMS roughness value between 6 and 8 Å, which would have completely damped any gentle Kiessig fringes observed in the XRR curves (*cf.* Fig. 4). That is, our XRR data could not be fitted using the RMS roughness values associated with surface cylinders (*cf.* blue curves in Fig. 4). To explain different structures observed using different techniques, we would like to suggest that the surfactant layers in XRR and NR studies are unperturbed as compared with a layer under the AFM scanning nano-tip.

The essence of this suggestion is that such perturbations, originating from the normal force F_n and lateral force F_s exerted at the surfactant layers by the fast scanning nano-tip, could induce the formation of surface aggregates (*e.g.* cylinders of radius R and length L) from flat bilayers. To evaluate the feasibility of this suggestion, we may estimate the bending energy E_b required for bilayer-to-cylinder transformation process as[68] $E_b \sim \pi k_c L/R$, where k_c is the elastic bending constant of a lipid bilayer of order 10^{-20} J.[68] To the first approximation, this bending energy E_b is the work done ΔW by the application of a force f over the length L, and thus the force required to facilitate this bilayer-to-cylinder transformation is $f = d(\Delta W)/dL \sim \pi k_c/R$. Assuming $R \sim 2$ nm, this gives $f \sim 20$ pN or of that order, well below the typical values of the forces (F_n and F_s) experienced in the application of AFM imaging which are in the range of 100 pN or above. It can also be shown, from a simple estimation using the theory of contact mechanics, that the pressure exerted on the bilayers by the AFM nano-tip (of radius ~10 nm) is of the order 10^6 Pa or above. Thus, it is feasible that the scanning AFM tip would "perturb" the conformation of the surfactant surface layers. Furthermore, the elastic bending constant k_c should depend on the interactions, and thus the packing and density, of the surfactant molecules in the layer, which in turn is a function of the surfactant molecular architecture and concentration.

Our suggestion is also supported by the results from a recent study by Schniepp *et al.*[69] who investigated aqueous solutions of hexadecyltrimethylammonium chloride (C_{16}TAC) surfactants on gold surfaces using liquid-cell AFM. They demonstrated it was possible to change the orientation of C_{16}TAC surfactant aggregates in a controlled fashion, using a standard AFM probe. With this method they were able to convert all micelles in the investigated area completely into any of three preferred directions, *i.e.* symmetry axes, dictated by the gold lattice. In addition, a lateral force perpendicular to the scanning direction was observed whilst scanning the AFM tip across a layer of oriented surface micelles. This force was attributed to anisotropic friction between the probe and the C_{16}TAC aggregates and was hypothesized to be the origin of the observed tip-induced reorientation of the surface micelles.

Therefore we propose that the formation of C_{16}TAB bilayers observed from our XRR data analysis can be attributed to the fact that our surfactant films were unperturbed as compared with a layer under an AFM probe. Such proposal applies to all the C_nTABs analysed. We wish to comment that an image in reciprocal space is no less real than an AFM image, and that it is less easy to interpret and there may be limitations and ambiguities in the interpretation. However, this does not detract from the fact that the reciprocal space image is obtained without invasion and therefore we believe it is more likely to correspond to the true equilibrium state. Hence, it is tempting to term these intrinsic structures "*quiescent bilayers*".

Some of the AFM observations in the literature could be rationalized. For instance, Subramanian and Ducker[56] observed bilayers at low surfactant concentrations (below 0.5 cmc) but cylinders at higher surfactant concentrations. It could be that the surfactant bilayers were disordered and more fluid at lower concentrations, so that they could regain its equilibrium or quiescent morphology instantaneously; whereas when densely packed at above cmc, the stronger cohesive energy between the surfactant tails would preserve the induced structure over a much longer time. However, there are further questions that remain to be addressed. For instance, what is the correlation between the anisotropic orientations of surface aggregates (*e.g.* cylinders) and the direction and magnitude of the applied force in AFM imaging?

Another consideration in explaining the discrepancy between our interpretation of quiescent bilayers and the surface aggregates as observed by AFM is different time frames between XRR and AFM experiments. Our XRR data would have been collected typically ~2 hours after the solution is injected. However, as we have discussed in our introduction, AFM observations by Ducker *et al.*[2,6,7] and by Manne and Gaub[3] show that the initial organization of the surfactant aggregates (at 2 cmc) is in the form of flattened parallel cylinders, which then transform into a flat bilayer after some 24 hours. Our time frame would be more comparable to the initial stage of surfactant organisation in these previous studies where cylindrical surface aggregates are observed. Thus, the discrepancy between our quiescent bilayer and those by AFM imaging cannot be explained by different time frames of our XRR measurements.

3.4 Dependence of C_nTAB bilayer thicknesses and surface coverage on surfactant concentration and chain length *n*

Fig. 5(b) shows how the surface coverage of the C_nTAB layers varies as a function of surfactant concentration. Above the cmc, a full coverage of the surface by the hydrocarbon chains is evident for all the C_nTABs in the series. However, below the cmc, and at low surfactant concentrations, *i.e.* at 0.1 and 0.3 cmc, lower coverage is obtained, indicating the formation of patchy bilayers. In addition, below cmc, the coverage increases as the chain length increases. This points to hydrophobic interactions between the tails being the driving force for the adsorption and layer formation, as the hydrophobic energy increases ~1 to 2 k_BT with every CH_2 added to the chain.

As expected, the layer thickness increases with n at any particular concentration, as evident from Fig. 5(a). A significant result however is that a maximum thickness in the surfactant layer on mica is observed at ~1 cmc for all the C_nTABs. This is somewhat counter-intuitive. Two effects upon increasing the surfactant concentration above cmc should be considered. (1) The associated increase in the number density of micelles in the solution, which would lead to closer distance between micelles and thus affect the inter-micelle interactions. However, at 3 and 5 cmc, the micelle number density remains very low, well below the concentration at which mesophases would begin to form where such inter-micelle interactions would become a significant contribution to the total chemical potential. Thus, it is unclear if this additional inter-micelle interaction could explain observed thickness-maximum at around cmc. (2) The effective ionic strength in the solution would increase due to dissociation of the cationic surfactants. The Debye screening length κ^{-1} would scale as $C^{-1/2}$, where C is the surfactant concentration, and thus at 2 and 5 cmc, κ^{-1} would be compressed to 70% and 40%, respectively, of that at 1 cmc. This would reduce the headgroup repulsion and in turn makes it easier for surfactant molecules to come together, similar to the effect of adding salt. However, one would expect this should encourage surfactant adsorption.

Another possibility is that this thickness reduction is a result of molecular conformation corresponding to minimized chemical potential as the surfactant concentration increases above cmc. We may attempt to explain this by considering the thermodynamic equilibrium between the surfactant molecules in the surface bilayer and in the micelle, *i.e.* the electrochemical potential per molecule must be the same everywhere. One relevant thermodynamic discussion is given by Evans and Wennerström,[70] and is summarised as follows. Considering N charged surfactant monomers S^+ in a micelle, with $(N - P)$ counterions C^- associated with the micelle and thus a net charge $+Pe$ (where e is the electronic charge 1.69×10^{-19} C), the surfactant chemical potential μ_{SC} has contributions from both of the ions as given by

$$\begin{aligned}\mu_{SC} &= \mu_{S^+} + \mu_{C^-} \\ &= \mu_S^\theta\,(\text{solvent}) + RT\ln[S^+] + \mu_{C^-}^\theta\,(\text{solvent}) + RT\ln[C^-] \\ &= \mu_{SC}^\theta\,(\text{solvent}) + RT\ln[S^+][C^-] \end{aligned} \quad (2)$$

where μ_{S^+} and μ_{C^-} are the chemical potentials of the surfactant ion and of the counterion, respectively, R is the gas constant, T is the absolute temperature, μ_S^θ, $\mu_{C^-}^\theta$ and μ_{SC}^θ are the standard chemical potentials of the surfactant ion, the counterion and the surfactant in the solution, respectively. Above the cmc, μ_{SC} is virtually independent of the total concentration, which implies that the product $[S^+][C^-]$ remains constant. Since a fraction of the counterions does not associate with the micelle, $[C^-]$ increases with total surfactant concentration. At the same time, for the product $[S^+][C^-]$ to stay constant, the free surfactant monomer concentration $[S^+]$ must decrease with increasing concentration, as must the chemical potential μ_{S^+} of the surfactant ion. Therefore, above the cmc, the adsorption on positively charged surfaces actually decreases as the surfactant concentration increases. In other words, some surfactant molecules would vacate surface sites and join micelles in the bulk. Consequently, maximum adsorption on the surface should occur close to the cmc, as we have observed.

This thermodynamic model however does not offer an intuitive physical insight on the structure of the bilayers, which we shall discuss below.

3.5 Bilayer structure: *interdigitation* and *tilting*

As already mentioned in the preceding sections, for all the C_nTABs at all concentrations, the bilayer thicknesses are below twice their fully extended monolayer thicknesses (including at 1 cmc where a maximum thickness is observed), but greater than the thicknesses of their fully extended monolayers. This might be due to partial interdigitation of the tails; or alternatively tilting of the tails which we have resorted to in discussing the bilayer structure at 1 cmc, and which has also been suggested by pervious NEXAS[67] and MD simulation studies.[55] We will further discuss the structural details of bilayers in this section.

At concentrations below cmc, the surface coverage is relatively low (*cf.* Fig. 5(b)). We expect that surfactant molecules are disordered and more fluid. It is thus possible for them to adopt a bilayer structure with partially interdigitated or interpenetrated tails (see the schematic in Fig. 5(a)). The idea is that the tails would be able to pervade such a volume with a relatively large cross-section area. As we shall argue shortly, it is this cross-section area that determines titling of the surface anchored bilayers.

At ~1 cmc and almost full surface coverage, we expect denser packing of the surfactant molecules and more rigid conformations of the tails. Partial interdigitation would lead to non-uniform hydrocarbon concentration in the tail region and consequently non-uniform pressure distribution in this region. In addition, it could also lead to an increase in the headgroup area, exposing hydrophobic tail region. Therefore, partial interdigitation is not likely. Instead, in line with previous NEXAS[67] and MD simulation studies,[55] we propose that the bilayers would adopt a tilted conformation, as schematically shown in Fig. 5 and also Fig. 6. The essence of this titled bilayer model is that the bilayer surface density is constrained by the charged mica surface sites, with a base area $A_s \sim 46.8$ Å^2.[71,72] At ~1 cmc, the surface sites are fully occupied. However, the cross-section area A_c of a fully stretched hydrocarbon with a zig-zag

backbone is ~18.8 Å^2.[73] To satisfy the packing constraint of one charged headgroup per site and pervade the space, the chains tilt so that the cross-section area (parallel to the mica basal plane) attains the value of $A_s \sim 46.8$ Å^2. This is illustrated in Fig. 6(d).

However, the actual cross-section area should depend on the packing of the chain, which in turn should depend on the chain length n. As the chain length increases, its hydrophobicity increases and its cmc decreases. The chemical potential per molecule upon micellisation, *i.e.* the chemical potential difference between a surfactant molecule in a micelle and in solution, is $\Delta\mu = k_BT\ln(\text{cmc})$. In Fig. 6(b), the projected cross-section area perpendicular to the chain length, $A_s\cos(\theta_t)$, is plotted against $\Delta\mu$ for the C_nTABs. It is evident that as n increases, $\Delta\mu$ becomes more negative (*i.e.* more favourable for micellisation) due to augmented hydrophobic attractions. This is expected to lead to denser packing of the tails, and thus a decrease in $A_s\cos(\theta_t)$, consistent with the trend in Fig. 6(b).

It should be commented that such tilting would lead to local structural anisotropy. However, it is conceivable that domains of the same tilt are present but on a macroscopic scale we do not expect any preference for any particularly orientation, so that the average $\langle\theta_t\rangle$ must be ~0. We note that such local domains have been previously observed for a diynoic acid Langmuir–Blodgett monolayer (with cadmium salt) on silicon.[74] XRR is not able to resolve such in plane structural information, and

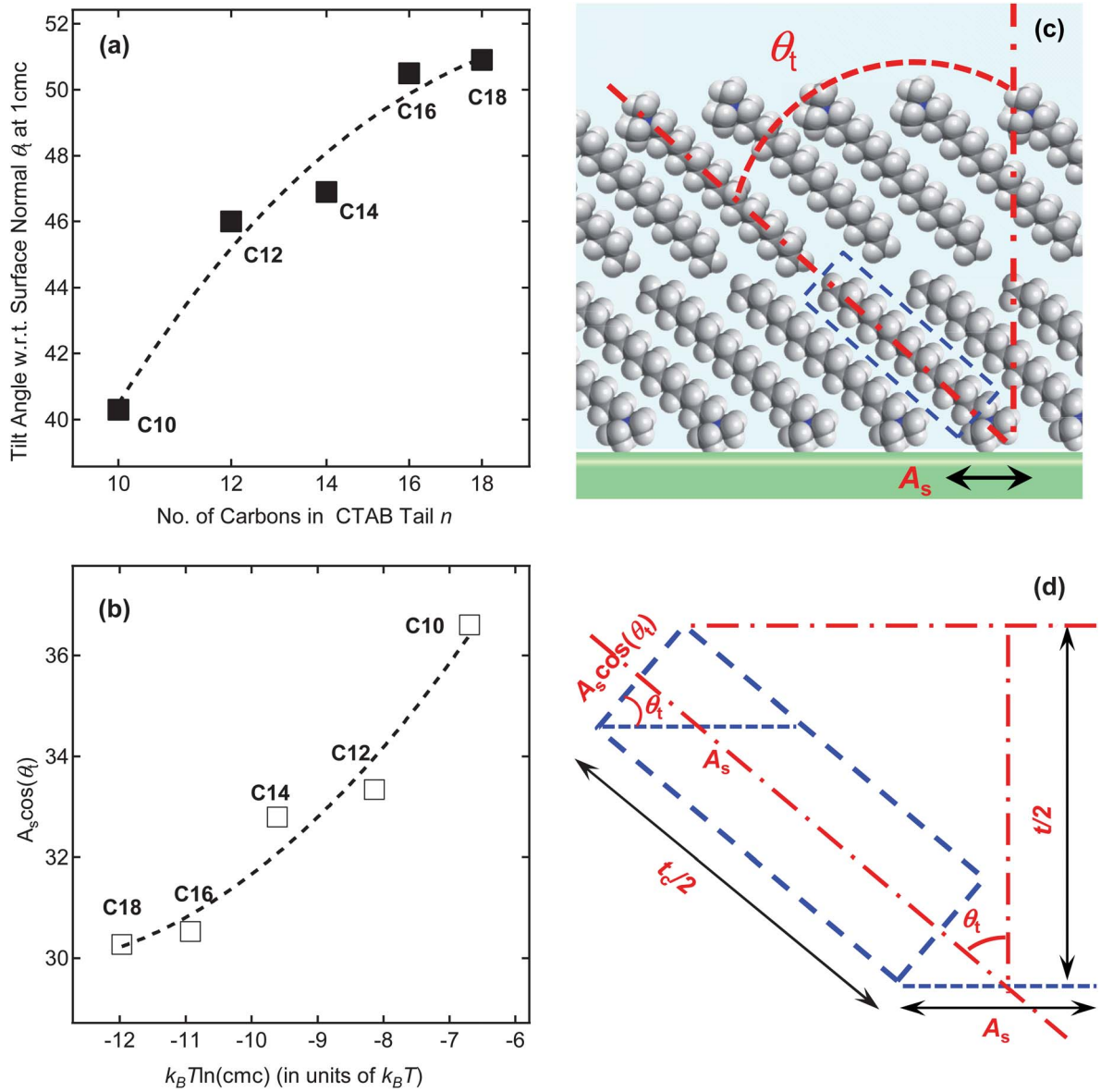

Fig. 6 (a) Tilt angle θ_t with respect to (w.r.t.) the surface normal of the adsorbed C_nTAB bilayer at ~1 cmc as a function of the number of hydrocarbons n in the C_nTAB tail. The dashed curves are a guide for the eye. (b) Cross-section area $A_s\cos(\theta_t)$ of the hydrocarbon tails for different C_nTAB bilayers *vs.* their chemical potential of micellisation per molecule $k_BT\ln(\text{cmc})$. (c) A schematic representation of a proposed tilted bilayer with a tilt angle θ_t. Each surfactant molecule occupies a mica surface site of area $A_s = 46.8$ Å^2. (d) An enlarged view of the tilt molecular geometry in (c).

grazing incidence surface X-ray scattering might be a suitable technique for ascertaining the presence such domains.

As the surfactant concentration further increases, the thermodynamic model states that the surface concentration of the surfactant molecules [S^+] would decrease. This would recover certain fluidity of the chains and thus permit interdigitation to occur, as in the case of below cmc, as shown schematically in Fig. 5(a). One possible experiment to verify this structural change from below cmc, to 1 cmc and to above cmc is to directly measure the forces required to fuse the bilayers as a function of surfactant concentration. We expect that a maximum fusion force would be required at ~1 cmc, due to the structural integrity of the tilted bilayer at 1 cmc.

4 Summary and concluding remarks

Using a liquid cell that employs a simple "bending mica" method, we have applied synchrotron XRR to study the structure of the adsorbed layers of C_nTABs at the mica–water interface, obtaining quantitative information on the layer thickness, surface coverage and interfacial roughness. Such structural details have not been obtained previously for surfactant layers at the mica–water interface, and thus provide the first direct comparison with results obtained by other experimental techniques and computer simulation studies. The results from these previous studies have presented different and sometimes contradicting morphologies and structures of self-assembled C_nTAB surfactant aggregates at surfaces. In particular, AFM imaging has unveiled a number of aggregate morphologies ranging from surface micelles to cylinders; whereas neutron reflectivity has reported patchy or full bilayers at the silica–water interface.

Our XRR results could not be fitted with surface structures of cylinders or spheres; instead, they could be consistently described by a bilayer model. We suggest that this is due to the fact that our surfactant films are unperturbed or "quiescent" as compared with a surfactant layer under an AFM scanning probe.

A second significant result, as shown in Fig. 5(a), is that the surfactant layer thickness exhibits a maximum at ~1 cmc for all the C_nTABs investigated. We propose that the surfactants form partially interdigitated bilayers below cmc, due to relatively fluid and disordered chains. At ~1 cmc, the surface sites of mica become densely and fully occupied, and surfactant molecules tilt w.r.t. the surface normal, to satisfy the packing constraints set by the area of the mica surface site, consistent with NEXAS[67] and MD simulation studies.[55] The tilt angle θ_t is observed to increase with the chain length n, and we have explained this by correlating θ_t with the chemical potential of micellisation per molecule, $\Delta\mu = k_BT\ln(\text{cmc})$. That is, the chains become more densely packed as the hydrophobic driving force increases with the chain length. Thus, the chains have to tilt more to satisfy the above surface-site packing constraint. As the surfactant concentration increases further above cmc, we propose that some surfactant molecules would desorb from the surface, consistent with a thermodynamic model due to Evans and Wennerström,[70] and consequently the bilayers recover fluidity and in turn the interdigitated structure.

Here we have focused on C_nTABs where n is even. In a report to follow, we will discuss the difference in the surface structures between C_nTABs with even- and odd-numbered hydrocarbons.

Acknowledgements

We are indebted to P. Thompson and S. Brown at ESRF BM28 and Chris Nicklin at I07 of the Diamond Light Source (UK) for their invaluable technical assistance and advice. Funding from the EPSRC (EP/H034862/1), European Research Council, the Royal Society (UK), the John Fell Fund (Oxford), the Taiho Kogyo Tribology Research Foundation (TTRF), the European Research Council and the European for Cooperation in Science and Technology (CMST COST) Action CM1101 "Colloidal Aspects of Nanoscience for Innovative Processes and Materials", Marie Curie Initial Training Network (MCITN) on "NanoS3" is gratefully acknowledged. F.S., G.A.P., P.T.C. and T.G.D. acknowledge support from the School of Chemistry, University of Bristol. The surface tension data for C_{16}TAB and C_{18}TAB were obtained at the Diamond I07 Chemistry Lab by P.L. W.H.B would like to thank K. Edler (University of Bath) for a helpful discussion.

References

1 M. J. Rosen, *Surfactants and Interfacial Phenomena*, Wiley-Interscience, Hoboken, N.J., 2004.
2 J. F. Liu and W. A. Ducker, *J. Phys. Chem. B*, 1999, **103**, 8558–8567.
3 S. Manne and H. E. Gaub, *Science*, 1995, **270**, 1480–1482.
4 W. A. Ducker and L. M. Grant, *J. Phys. Chem.*, 1996, **100**, 11507–11511.
5 L. M. Grant and W. A. Ducker, *J. Phys. Chem. B*, 1997, **101**, 5337–5345.
6 W. A. Ducker and E. J. Wanless, *Langmuir*, 1999, **15**, 160–168.
7 R. E. Lamont and W. A. Ducker, *J. Am. Chem. Soc.*, 1998, **120**, 7602–7607.
8 B. G. Sharma, S. Basu and M. M. Sharma, *Langmuir*, 1996, **12**, 6506–6512.
9 H. N. Patrick, G. G. Warr, S. Manne and I. A. Aksay, *Langmuir*, 1999, **15**, 1685–1692.
10 F. Zhao, Y. Du, P. Yang, X. Li and J. Tang, *Sci. China, Ser. B*, 2005, 48.
11 M. W. Cao and X. L. Wang, *J. Dispersion Sci. Technol.*, 2009, **31**, 38–43.
12 O. Teschke, G. Ceotto and E. F. de Souza, *J. Vac. Sci. Technol., B*, 2000, **18**, 1144–1150.
13 W. Han, *Ultramicroscopy*, 2008, **108**, 1009–1012.
14 A. Blom, F. P. Duval, L. Kovacs, G. G. Warr, M. Almgren, M. Kadi and R. Zana, *Langmuir*, 2004, **20**, 1291–1297.
15 Y. B. Hou, M. W. Cao, M. T. Deng and Y. L. Wang, *Langmuir*, 2008, **24**, 10572–10574.
16 C. H. See and J. H. O'Haver, *Colloids Surf., A*, 2004, **243**, 169–183.
17 B. Y. Li, M. Fujii, K. Fukada, T. Kato and T. Seimiya, *Thin Solid Films*, 1998, **312**, 20–23.

18 W. H. Briscoe and R. G. Horn, *Langmuir*, 2002, **18**, 3945–3956.
19 W. H. Briscoe and J. Klein, *J. Adhes.*, 2007, **83**, 705–722.
20 J. Klein, *Nature*, 1980, **288**, 248–250.
21 P. Kékicheff, H. K. Christenson and B. W. Ninham, *Colloids Surf.*, 1989, **40**, 31–41.
22 P. Richetti and P. Kekicheff, *Phys. Rev. Lett.*, 1992, **68**, 1951–1954.
23 R. M. Pashley and J. N. Israelachvili, *Colloids Surf.*, 1981, **2**, 169–187.
24 R. M. Pashley, P. M. McGuiggan, R. G. Horn and B. W. Ninham, *J. Colloid Interface Sci.*, 1988, **126**, 569–578.
25 R. M. Pashley and B. W. Ninham, *J. Phys. Chem.*, 1987, **91**, 2902–2904.
26 J. L. Parker, *Prog. Surf. Sci.*, 1994, **47**, 205–271.
27 C. A. Helm, J. N. Israelachvili and P. M. McGuiggan, *Science*, 1989, **246**, 919–922.
28 M. Rutland, A. Waltermo and P. Claesson, *Langmuir*, 1992, **8**, 176–183.
29 W. H. Briscoe, S. Titmuss, F. Tiberg, R. K. Thomas, D. J. McGillivray and J. Klein, *Nature*, 2006, **444**, 191–194.
30 J. N. Israelachvili and G. E. Adams, *Nature*, 1976, **262**, 774–776.
31 P. I. Hanson, R. Roth, H. Morisaki, R. Jahn and J. E. Heuser, *Cell*, 1997, **90**, 523–535.
32 S. B. Velegol, B. D. Fleming, S. Biggs, E. J. Wanless and R. D. Tilton, *Langmuir*, 2000, **16**, 2548–2556.
33 J. C. Schulz, G. G. Warr, P. D. Butler and W. A. Hamilton, *Phys. Rev. E: Stat., Nonlinear, Soft Matter Phys.*, 2001, 63.
34 J. N. Israelachvili and R. M. Pashley, *J. Colloid Interface Sci.*, 1984, **98**, 500–514.
35 G. A. Pilkington and W. H. Briscoe, *Adv. Colloid Interface Sci.*, 2012, **179–182**, 68–84.
36 C. Tanford, *J. Phys. Chem.*, 1972, **76**, 3020–3024.
37 G. Fragneto, R. K. Thomas, A. R. Rennie and J. Penfold, *Langmuir*, 1996, **12**, 6036–6043.
38 A. R. Rennie, E. M. Lee, E. A. Simister and R. K. Thomas, *Langmuir*, 1990, **6**, 1031–1034.
39 J. Penfold, I. Tucker, J. Petkov and R. K. Thomas, *Langmuir*, 2007, **23**, 8357–8364.
40 D. C. McDermott, J. McCarney, R. K. Thomas and A. R. Rennie, *J. Colloid Interface Sci.*, 1994, **162**, 304–310.
41 E. S. Pagac, D. C. Prieve and R. D. Tilton, *Langmuir*, 1998, **14**, 2333–2342.
42 R. Atkin, V. S. J. Craig and S. Biggs, *Langmuir*, 2000, **16**, 9374–9380.
43 R. Atkin, V. S. J. Craig, E. J. Wanless and S. Biggs, *J. Colloid Interface Sci.*, 2003, **266**, 236–244.
44 K. Eskilsson and V. V. Yaminsky, *Langmuir*, 1998, **14**, 2444–2450.
45 E. M. A. Pereira, D. F. S. Petri and A. M. Carmona-Ribeiro, *J. Phys. Chem. B*, 2006, **110**, 10070–10074.
46 P. Wangnerud, D. Berling and G. Olofsson, *J. Colloid Interface Sci.*, 1995, **169**, 365–375.
47 L. Lajtar, J. Narkiewiczmichalek and W. Rudzinski, *Langmuir*, 1994, **10**, 3754–3764.
48 K. H. S. Kung and K. F. Hayes, *Langmuir*, 1993, **9**, 263–267.
49 P. K. Singh, J. J. Adler, Y. I. Rabinovich and B. M. Moudgil, *Langmuir*, 2001, **17**, 468–473.
50 Y. L. Chen, S. Chen, C. Frank and J. Israelachvili, *J. Colloid Interface Sci.*, 1992, **153**, 244–265.
51 A. Meleshyn, *Langmuir*, 2009, **25**, 6250–6259.
52 R. A. Johnson and R. Nagarajan, *Colloids Surf., A*, 2000, **167**, 21–30.
53 A. Meleshyn, *Langmuir*, 2009, **25**, 881–890.
54 H. Heinz, R. A. Vaia, R. Krishnamoorti and B. L. Farmer, *Chem. Mater.*, 2007, **19**, 59–68.
55 H. Heinz, H. J. Castelijns and U. W. Suter, *J. Am. Chem. Soc.*, 2003, **125**, 9500–9510.
56 V. Subramanian and W. Ducker, *J. Phys. Chem. B*, 2001, **105**, 1389–1402.
57 W. J. Lokar and W. A. Ducker, *Langmuir*, 2002, **18**, 3167–3175.
58 R. Podgornik and V. A. Parsegian, *J. Phys. Chem.*, 1995, **99**, 9491–9496.
59 H. K. Christenson and V. V. Yaminsky, *Colloids Surf., A*, 1997, **130**, 67–74.
60 V. V. Yaminsky, B. W. Ninham, H. K. Christenson and R. M. Pashley, *Langmuir*, 1996, **12**, 1936–1943.
61 V. Yaminsky, C. Jones, F. Yaminsky and B. W. Ninham, *Langmuir*, 1996, **12**, 3531–3535.
62 W. H. Briscoe, M. Chen, I. E. Dunlop, J. Klein, J. Penfold and R. M. J. Jacobs, *J. Colloid Interface Sci.*, 2007, **306**, 459–463.
63 W. H. Briscoe, F. Speranza, P. Li, O. Konovalov, L. Bouchenoire, J. van Stam, J. Klein, R. M. J. Jacobs and R. K. Thomas, *Soft Matter*, 2012, **8**, 5055–5068.
64 J. R. Lu, Z. X. Li, J. Smallwood, R. K. Thomas and J. Penfold, *J. Phys. Chem.*, 1995, **99**, 8233–8243.
65 S. D. Brown, L. Bouchenoire, D. Bowyer, J. Kervin, D. Laundy, M. J. Longfield, D. Mannix, D. F. Paul, A. Stunault, P. Thompson, M. J. Cooper, C. A. Lucas and W. G. Stirling, *J. Synchrotron Radiat.*, 2001, **8**, 1172–1181.
66 L. Cheng, P. Fenter, K. L. Nagy, M. L. Schlegel and N. C. Sturchio, *Phys. Rev. Lett.*, 2001, **87**, 156103.
67 D. Brovelli, W. R. Caseri and G. Hähner, *J. Colloid Interface Sci.*, 1999, **216**, 418–423.
68 E. Evans and W. Rawicz, *Phys. Rev. Lett.*, 1990, **64**, 2094–2097.
69 H. C. Schniepp, D. A. Saville and I. A. Aksay, *Langmuir*, 2008, **24**, 626–631.
70 F. Evans and H. Wennerström, *The colloidal domain: where physics, chemistry, biology, and technology meet*, Wiley, New York, 1999.
71 E. W. Radoslovich, *Acta Crystallogr.*, 1960, **13**, 919–932.
72 N. Guven, *Zeitschrift Fur Kristallographie Kristallgeometrie Kristallphysik Kristallchemie*, 1971, **134**, 196–212.
73 K. Okuyama, Y. Soboi, N. Iijima, K. Hirabayashi, T. Kunitake and T. Kajiyama, *Bull. Chem. Soc. Jpn.*, 1988, **61**, 1485–1490.
74 H. G. Braun, H. Fuchs and W. Schrepp, *Thin Solid Films*, 1988, **159**, 301–314.